Supplementary Information

Aluminum oxide nanoparticle films deposited from a nonthermal plasma: synthesis, characterization, and crystallization

Zhaohan Li,[‡] Parker R. Wray,[⊥] Magel P. Su,[⊥] Qiaomiao Tu,[‡] Himashi P. Andaraarachchi,[‡] Yong Jin Jeong,[‡,1] Harry A. Atwater,[⊥] Uwe R. Kortshagen*[‡]

[‡]*Department of Mechanical Engineering, University of Minnesota, 111 Church St. SE, Minneapolis, Minnesota 55455, United States*

[⊥]*California Institute of Technology, Thomas J. Watson Laboratories of Applied Physics, MS 128-95, Pasadena, California 91125 United States*

**Corresponding author. Email: kortshagen@umn.edu*

[1] *Current address: Department of Materials Science & Engineering, Korea National University of Transportation, 50 Daehak-ro, Daesowon-myeon, Chungju, 27469, Republic of Korea*

Supplementary Figures

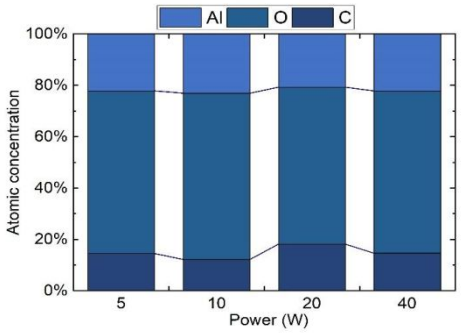

Figure S1. Atomic concentration in samples from type B reactor obtained by XPS with power varying from 5 W to 40 W.

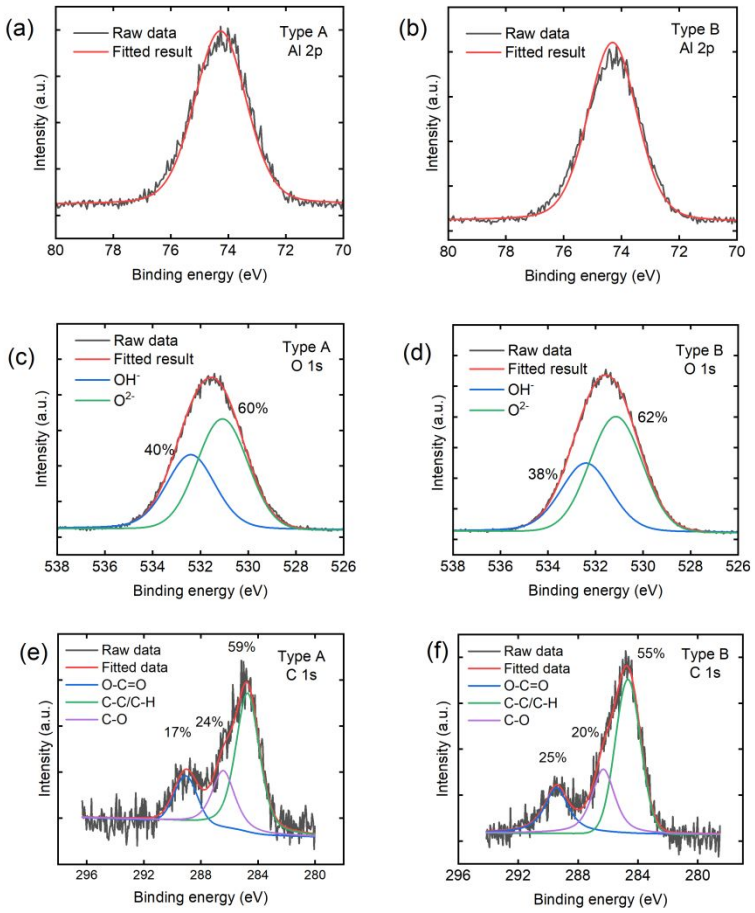

Figure S2. XPS high resolution spectra of Al 2p peak (a,b), O 1s peak (c,d) and C 1s peak (e,f) for AlO_x nanoparticle samples from type A and type B reactors. The peak corresponding to adventitious carbon is shifted to 284.8 eV as a reference.

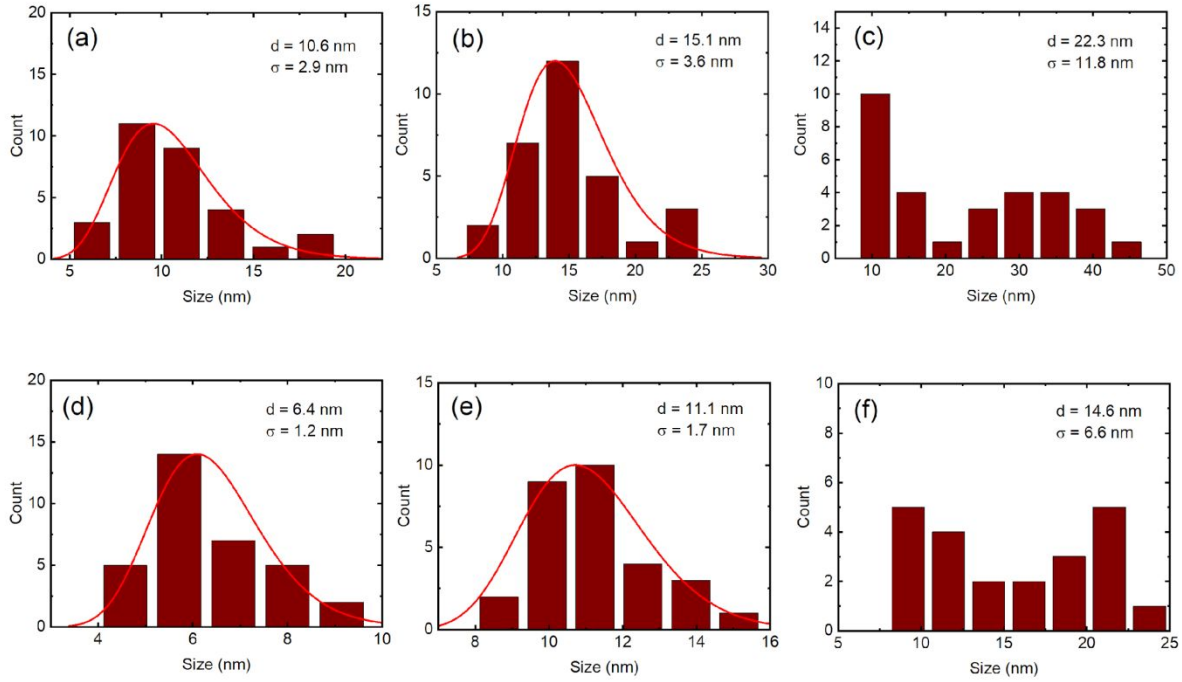

Figure S3. (a)–(f) Size distributions corresponding to the TEM images in Figures 3 (a) to (f).

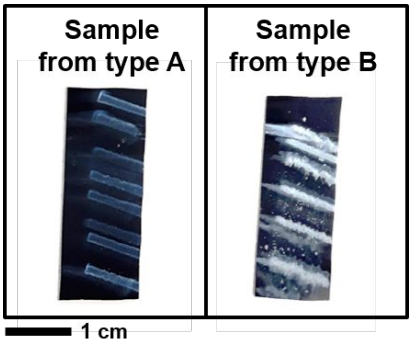

Figure S4. Photograph showing AlO_x nanoparticles deposited from type A and type B reactors for same period of time.

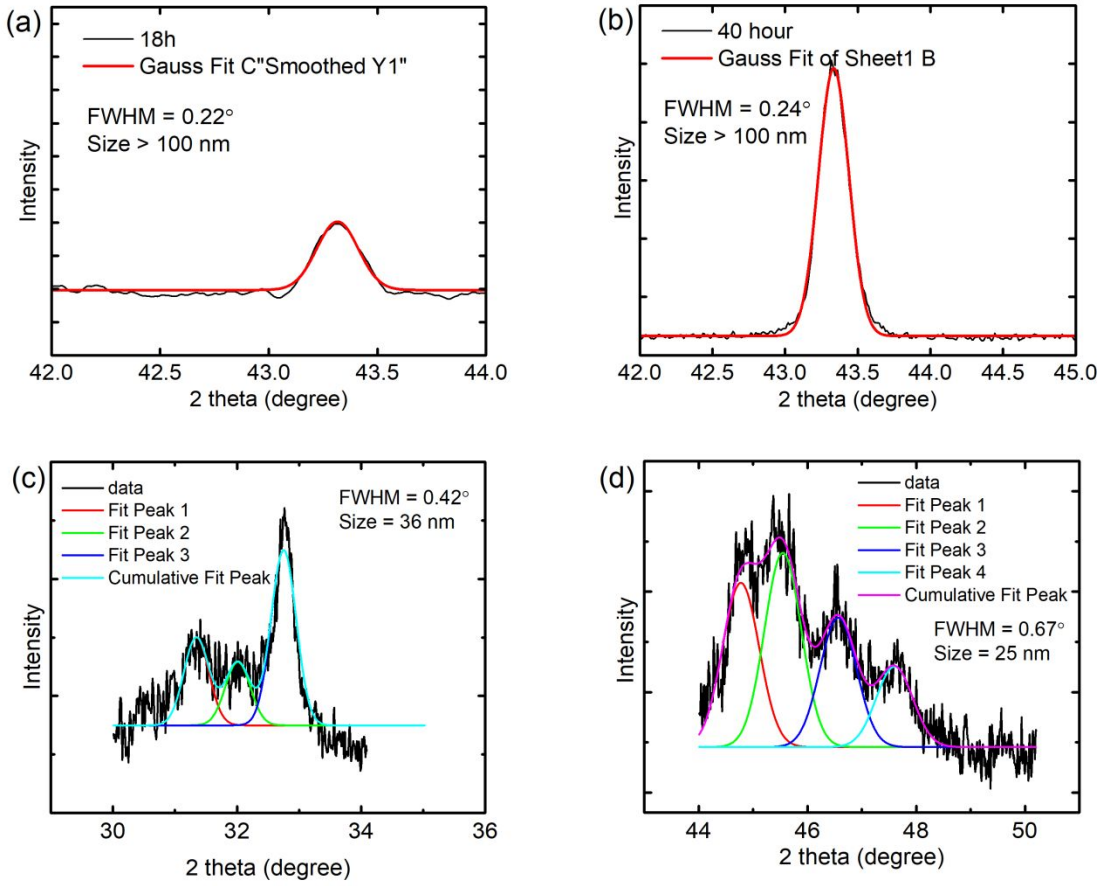

Figure S5. Scherrer fittings of XRD patterns (λ = 1.54 Å) of AlO_x nanoparticles from type B reactor after heating at 1100 ˚C for 18 h and for 40 h. To obtain size estimates for the α-phase and θ-phase individually, we choose non-overlapping peaks from the two phases. For the α-phase, (113) peaks were fitted (a,b). For θ-phase, peaks around 30-34˚ (c) and 44-50˚ (d) were fitted. Instrumental broadening was accounted for by subtracting the FWHM of the nearest peak of the LaB_6 standard sample, Figure S1. In the Scherrer equation, a shape factor of 0.89 was used. As the widths of α-phase peaks are close to those of the LaB_6 standard sample indicating large crystallite sizes, a rough size estimate of >100 nm is quoted in the main text.

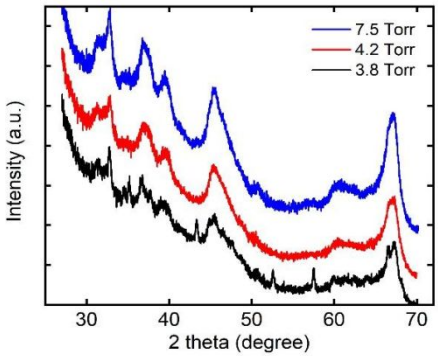

Figure S6. XRD patterns of samples from type B reactor for three nanoparticle sizes, obtained by varying the gas pressure, after annealing at 1100˚C for 18 hours. Only the smallest particles with about 6 nm size show the appearance of the α-phase.

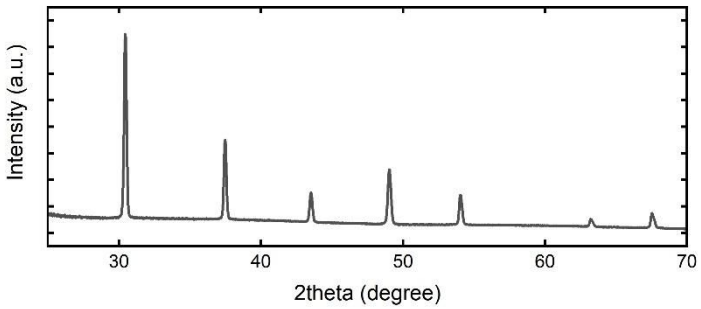

Figure S7. XRD pattern from a standard LaB_6 sample taken using a Bruker D8 Discover 2D X-ray diffractometer. This pattern is used as a reference to correct for instrument broadening.

Permittivity modeling of amorphous aluminum oxide nanoparticle films

The film's homogenized permittivity (ε_{eff}) can be represented by a wavelength dependent scalar. We model ε_{eff} using the Bruggeman mixing formula

$$f_{AlO_x}\frac{\varepsilon_{AlO_x}-\varepsilon_{eff}}{\varepsilon_{eff}+k(\varepsilon_{AlOx}-\varepsilon_{eff})}+\ (1-f_{AlO_x})\frac{\varepsilon_{air}-\varepsilon_{eff}}{\varepsilon_{eff}+k(\varepsilon_{air}-\varepsilon_{eff})}=0\#(1)$$

where ε_{AlOx} and ε_{air} are the permittivity of the nanoparticles and air, respectively; f_{AlOx} ($=22.3\pm0.33\%$ for type A and $19.4\pm0.11\%$ for type B) volume fill fraction of the AlO_x

nanoparticles; and k ($= 0.261 \pm 0.005$ for type A and 0.407 ± 0.006 for type B) is the depolarizing factor 1. ε_{AlOx} is modeled as

$$\frac{\varepsilon_{AlO_x}(E)}{\varepsilon_o} = \varepsilon_\infty + \varepsilon_{pole1} + \varepsilon_{pole2} + \sum_{n=1}^{11} \varepsilon_{Gauss_n}(E) \#(2)$$

Where ε_o is the permittivity of free space and ε_∞ ($= 3.09 \pm 0.01$ for type A and 2.97 ± 0.02 for type B) is the infinite frequency permittivity. The complex part of the Gaussian oscillators $\left(\varepsilon_{Gauss_n} = \varepsilon_{1n}(E) + i\varepsilon_{2n}(E)\right)$ are given by

$\varepsilon_{2n}(E) = A_n e^{-\left(\frac{E-E_n}{\sigma_n}\right)^2} - A_n e^{-\left(\frac{E+E_n}{\sigma_n}\right)^2}$, $\sigma_n = \frac{Br_n}{2\sqrt{\ln(2)}}$,#(3)where Br_n is the full-width at half-maximum, which accounts for spectral broadening. The real part of the permittivity is given by the Kramers-Kronig relation

$$\varepsilon_{1n}(E) = \frac{2}{\pi} P \int_0^\infty \frac{\xi \varepsilon_{2n}(\xi)}{\xi^2 - E^2} d\xi, \#(4)$$

where P is the principle value. Table 1 and Table 2 give the fit parameters of the Gaussian oscillators for the amorphous Al_2O_3 nanoparticle films from type A and type B reactors, respectively.

Type A	*Gaussian Oscillator Fit*			*Literature Values*	
Vibration	*Amplitude*	*Broadening [cm^{-1}]*	*Frequency [cm^{-1}]*	*Frequency [cm^{-1}]*	*Ref.*
AlO_6, AlO_4 Deformations	1.0340	83.221	344.27	322−326	[1][2]
AlO_6 stretching	4.6977	408.32	475.78	482−491	[1]
AlO_4 stretching	0.3357	107.70	851.46	902−880	[1][3][4]
Al−OH sym/asym	0.6933	341.47	1027.5	1072−1160	[1][5]
H_2O deformations/ vibrations	0.22815	92.908	1410.6	1375	[1]

H−O−H bend	0.31668	159.19	1535.8	1600	[4]
$-COO^-$	0.0783	74.000	1655.8	1300−1850	[2]
	0.05905	1700.8	2355.7		
Al−OH stretching	0.19133	618.98	3207.7	3250−3600	[2][4]
O−H stretching	0.20091	278.01	3429.0	3400-3600	[1][2][5]
Al−OH stretching	0.0719	162.00	3523.7	3250−3600	[2][4]

Table 1. Gaussian oscillator parameters used to reconstruct the permittivity of nanoparticles from type A reactor. Phonon resonance type (first column), amplitude (second column), spectral broadening (third column) and resonant frequency (fourth column) of the Gaussian oscillators used to calculate the AlO_x particle permittivity from Mueller matrix data. The fifth column gives the resonant frequency range expected from previous literature reports. Citations for the expected frequency range are in the sixth column.

Type B	*Gaussian Oscillator Fit*			*Literature Values*	
Vibration	*Amplitude*	*Broadening [cm^{-1}]*	*Frequency [cm^{-1}]*	*Frequency [cm^{-1}]*	*Ref.*
AlO_6, AlO_4 Deformations	2.5049	109.52	318.72	322−326	[1][2]
AlO_6 stretching	4.0194	320.53	531.22	482−491	[1]
AlO_4 stretching	0.4802	100.47	837.05	902−880	[1][3][4]
Al−OH sym/asym	0.78315	397.17	966.53	1072−1160	[1][5]

H_2O deformations/ vibrations	0.26118	98.502	1403.0	1375	[1]
H−O−H bend	0.37889	140.14	1520.6	1600	[4]
$-COO^-$	0.0780	74.000	1635.8	1300−1850	[2]
	0.0759	1883.7	2237.9		
Al−OH stretching	0.1738	559.78	3129.3	3250−3600	[2][4]
O−H stretching	0.3324	304.69	3406.2	3400-3600	[1][2][5]
Al−OH stretching	0.1019	162.53	3607.7	3250−3600	[2][4]

Table 2. Gaussian oscillator parameters used to reconstruct the permittivity of nanoparticles from type B reactor. Phonon resonance type (first column), amplitude (second column), spectral broadening (third column) and resonant frequency (fourth column) of the Gaussian oscillators used to calculate the AlO_x particle permittivity from Mueller matrix data. The fifth column gives the resonant frequency range expected from previous literature reports. Citations for the expected frequency range are in the sixth column.

References

(1) Boumaza, A.; Favaro, L.; Lédion, J.; Sattonnay, G.; Brubach, J.; Berthet, P.; Huntz, A.;Roy, P.; Tétot, R. Transition alumina phases induced by heat treatment of boehmite: an X-ray diffraction and infrared spectroscopy study. *J. Solid State Chem.* **2009**, *182*, 1171–1176.

(2) Catherine, Y.; Talebian, A. Plasma deposition of aluminum oxide films. *J. Electron. Mater.* **1988**, *17*, 127–134.

(3) Zagrajczuk, B.; Dziadek, M.; Olejniczak, Z.; Sulikowski, B.; Cholewa-Kowalska, K.; Laczka, M. Structural investigation of gel-derived materials from the SiO_2–Al_2O_3 system. *J. Mol. Struct.* **2018**, *1167*, 23–32.

(4) Wäckelgård, E. The experimental dielectric function of porous anodic alumina in the infrared region; a comparison with the Maxwell-Garnett model. *J. Phys.: Condens. Matter* **1996**, *8*, 4289.

(5) Liu, C.; Shih, K.; Gao, Y.; Li, F.; Wei, L. Dechlorinating transformation of propachlor through nucleophilic substitution by dithionite on the surface of alumina. *J. Soils Sediments* **2012**, *12*, 724–733.